PHYSICAL REVIEW D VOLUME 16, NUMBER 9 1 NOVEMBER 1977

Polarizations of A mesons produced in $\pi^{\pm}p$ collisions

Richard A. Morrow
Bennett Hall, University of Maine, Orono, Maine 04473
(Received 29 November 1976)

A Regge model with Pomeron and f-meson exchanges is developed for A_1, A_2, and A_3 meson production in π^+p collisions. The residues used are derived from a previously developed model of symmetric vertex couplings. Fits to total cross sections, differential cross sections, and spin-density matrix elements (SDME) for pion laboratory momenta up to 40 GeV/c are displayed. A discrepancy with the data is found in the sign of the SDME $\mathrm{Re}\rho_{12}$ for A_2 production and $\mathrm{Re}\rho_{10}$ for A_3 production.

I. INTRODUCTION

Of the three A mesons listed in the Particle Data Group tables[1] only the A_2 (1310 MeV/c^2, $\Gamma = 102$ MeV, $J^P = 2^+$), with dominant decay into $\rho\pi$, is established as a *resonance*. Both the A_1 (1100 MeV/c^2, $\Gamma \sim 300$ MeV, $J^P = 1^+$) with sole observed decay into $\rho\pi$ and the A_3 (1640 MeV/c^2, $\Gamma \sim 300$ MeV, $J^P = 2^-$) with sole observed decay into $f\pi$ appear as broad enhancements just above the $\rho\pi$ and $f\pi$ thresholds, respectively, in 3π final states. The A_1 and A_3 are not established as resonances because their respective production amplitudes do not exhibit a *large* phase change[2-7] as the $\rho\pi/f\pi$ effective mass transverses the enhancement. Furthermore, the neutral members of the isotriplets A_1 and A_3 have never been detected.[8] These features have led to the currently popular view that the threshold enhancements identified as the A_1 and A_3 are simply kinematic in origin.

Successful models of A-meson production must take into account a vast amount of detailed information made available by the applications of the University of Illinois partial-wave analysis program[9] to data from the reactions $\pi^{\pm}p \to (\pi^{\pm}\pi^+\pi^-)p$ at pion laboratory momenta up to 40 GeV/c (see Table I).[2-7,10] Total cross sections, differential cross sections, t-channel spin density matrix elements (SDME), and phase differences between various production amplitudes are available. The most successful fits to these data for A_1 and A_3 production have used a Reggeized Deck model[11,12] which turns out to work well for the A_1, but less so for the A_3. No detailed fits of the A_2 data have yet been published. Even the papers on the A_1 and A_3 fits do not report on the SDME but are more concerned with a proper accounting of the dominant helicity amplitude in each case.

In contrast to existing presentations, all three production processes are treated on an equal footing in the present paper using a simple t-channel description which involves Pomeron and f exchanges. An attempt is made to fit total cross sections, differential cross sections, and SDME of the A mesons over an incident-pion-laboratory-momentum range from 10 GeV/c to 40 GeV/c. The view adopted at the outset is that each of the A mesons, having a well-defined spin and parity, is also describable by a local quantum field; in short, that each can be treated as a localized entity. A previously developed symmetric-coupling model (SCM)[13] of vertex functions is used to construct Reggeized amplitudes for the processes $\pi p \to Ap$. A few parameters in each amplitude are adjusted in an attempt to fit as much data as possible.

The main concern in this approach is with a proper accounting of the polarizations of the A mesons. There is no concern here with the important question of what happens to the A mesons once they are formed, e.g., with questions of phase variation of the production amplitudes as functions of the masses of the A mesons. The model is not meant to furnish a definitive description of A_1 and A_3 production. In these cases it could simply be simulating the Deck mechanism[14] inasmuch as the Deck amplitude predicts both the $\rho\pi$ and $f\pi$ threshold enhancements to have substantially unique spin and parity. In any case it is believed that the quantities calculated below should not be substantially different from those calculated using the Deck model.

The result of the present investigation is that all observables studied are found to agree reasonably well with the analyzed data except for two items: There is a serious conflict between theory and experiment with regard to the sign of the only nonvanishing (within statistics) off-diagonal SDME for both $J = 2$ mesons. Theory predicts that $\mathrm{Re}\rho_{12}$ for the A_2 and $\mathrm{Re}\rho_{10}$ for the A_3 are negative. Experiment gives positive values for these two quantities. Theory and experiment are in agreement with regard to magnitudes, however. This disagreement in the sign of $\mathrm{Re}\rho_{10}$ for the A_3 is also deduced to be present in a Reggeized Deck description of A_3 production[11] and so transcends the par-

ticular model (SCM) of the residue function used in the present work. The basic reason for these disagreements is not apparent.

II. MODEL OF A-MESON PRODUCTION

As mentioned above, the model adopted involves Regge exchanges of the Pomeron (P) and the f meson. That the Pomeron is needed follows from the observed slow decrease of the total cross section, $\sigma(s)$, with increasing $\pi^{\pm}p$ center-of-mass energy, $\sqrt{s}$ (Ref. 4):

$$\sigma(s)\alpha s^{2\alpha_0-2} \text{ with } \alpha_0 = 0.80\pm 0.03 \text{ for the } A_1$$
$$= 0.75\pm 0.03 \text{ for the } A_2$$
$$= 0.71\pm 0.10 \text{ for the } A_3 ,$$

where α_0 is the $t=0$ intercept of an effective trajectory.

Equality of A^+ and A^- production cross sections[4,7] further indicates that exchange of Reggeons odd under charge conjugation are unimportant. It is then supposed that the f meson is the most important contributor besides the Pomeron.

The t-channel description of the production processes is illustrated in Fig. 1. Letting σ, τ, and ν denote the helicities of proton, antiproton, and A meson, respectively, each amplitude is parametrized as

$$f^{\nu}_{\tau\sigma}(s,t) = G_P e^{Bt} e^{-i\phi_P}\mathfrak{M}^{(P)\nu}_{\tau\sigma}(s,t) + G_f\mathfrak{M}^{(f)\nu}_{\tau\sigma}(s,t) , \quad (1)$$

where $\mathfrak{M}^{(i)\nu}_{\tau\sigma}(s,t)$ for $i=P,f$ is the t-channel amplitude involving Reggeon i and is represented by the appropriate graph of Fig. 1. In constructing these latter amplitudes the assumption is made that the Pomeron has a coupling to external particles like that of the f meson[15] and differs from the f meson primarily in the behavior of its trajectory. Additional differences between the Pomeron and the f meson are expressed by the parameters G_P, B, and ϕ_P in (1).

TABLE I. Data source references for total cross sections (σ), differential cross sections ($d\sigma/dt$), and t-spin density matrix elements (SDME).

Reference number	Mesons	Observables used	Incident pion momentum
2	A_3^-	$d\sigma/dt$, SDME	11–25 GeV/c
3	A_2^-	$d\sigma/dt$	11–25 GeV/c
4	A_1^-, A_2^-, A_3^-	σ	5–40 GeV/c
	A_1^-, A_2^-, A_3^-	$d\sigma/dt$, SDME	25, 40 GeV/c
5	A_1^+, A_2^+	σ, $d\sigma/dt$	13 GeV/c
6	A_3^+	σ, $d\sigma/dt$	13 GeV/c
	A_1^+, A_2^+, A_3^+	SDME	13 GeV/c
7	A_1^+, A_2^+, A_3^+	σ, $d\sigma/dt$	8, 16, 23 GeV/c
10	A_1^-	SDME	11–25 GeV/c

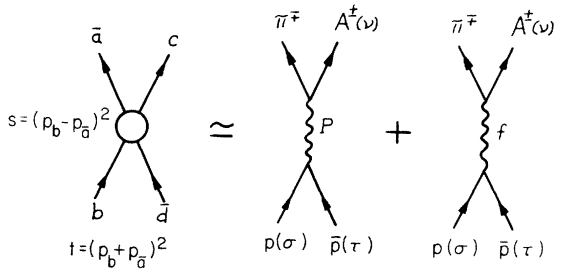

FIG. 1. The t-channel description of A-meson production, $p+\bar{p}\to\pi^{\mp}+A^{\pm}$, involving Pomeron ($P$) and f-meson exchange. Helicities are σ, τ, and ν.

In the context of the SCM the amplitudes $\mathfrak{M}^{(i)\nu}_{\tau\sigma}(s,t)$ are given by Eq. (33) of Ref. 13:

$$\mathfrak{M}^{(i)\nu}_{\tau\sigma}(s,t) = \bar{v}^{(i)}_B(\nu;\nu,0)^*\bar{v}^{(i)}_F(\mu;\tau,\sigma) \times \mathfrak{D}^{\alpha_i}_{\mu\nu}(\phi,\theta,-\phi)^* e^{-2i\sigma\phi}\frac{\pi}{2s_i}\frac{1+e^{-i\pi\alpha_i}}{\sin\pi\alpha_i}\alpha_i \quad (2)$$

(with $\mu\equiv\tau-\sigma$ and s_i = the inverse of the slope of the trajectory) in the t-channel center-of-mass frame with the momenta configuration shown in Fig. 2. The extra factor of α_i (the trajectory function of Reggeon i) inserted into (2) and not discussed in Ref. 13 is there to kill the ghost that would occur in the A_1 and A_3 cases for $t<0$ when $\alpha_i=0$. It should be removed in the A_2 case since a factor α_i is generated automatically in $\bar{v}_B(\nu;\nu,0)$ in this case. With regard to the factor $e^{-2i\sigma\phi}$, it comes from a factor $e^{-2i\Lambda_2^f\phi}$ which should be present in Eqs. (29), (33), and (38) of Ref. 13.

The vertex functions $\bar{v}$ of (2) were evaluated in Ref. 13 from a particular model of field couplings. As to the motivation underlying the SCM, suffice

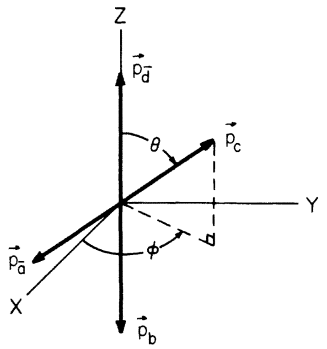

FIG. 2. The t-channel center-of-mass momenta configuration of the process illustrated in Fig. 1.

it to say that for vertices involving normal-parity bosons of any spins the function $\overline{V}_B$ is identical to that extracted from the dual amplitude B_{6°.[16] For vertices involving fermions or abnormal-parity particles $\overline{V}$ comes from appropriately generalized field couplings. All of the boson vertex functions, $\overline{V}_B$, used here agree with those extracted from dual models by Michael.[17]

Before the amplitudes (2) can be used to calculate observables, they must be analytically continued to the s channel. In the next section all of the vertex functions $\overline{V}$ are presented and the analytic continuation of the amplitudes is discussed. Readers uninterested in these details should skip to Sec. IV.

III. ANALYTIC CONTINUATION

Before displaying the vertex functions it will prove convenient to extract from them some common factors which are destined ultimately to be canceled by corresponding inverse factors from the $\mathfrak{D}$ function of (2). Thus, define

$$\overline{V}_B^{(i)}(\nu;\nu,0)\equiv(-i)^{\alpha_i}(\lambda_B/s_i t)^{\alpha_i/2}N_\nu\Gamma(\alpha_i+1)^{-1/2}V_B^{(i)}(\nu;\nu,0)\ ,$$

$$\overline{V}_F^{(i)}(\mu;\tau,\sigma)\equiv(-i)^{\alpha_i}(\lambda_F/s_i t)^{\alpha_i/2}N_\mu\Gamma(\alpha_i+1)^{-1/2}V_F^{(i)}(\mu;\tau,\sigma)\ ,$$

where

$$\lambda_B=\lambda(t,m_a^2,m_c^2)\ ,\quad \lambda_F=\lambda(t,m_b^2,m_d^2)\ ,$$

$$\lambda(x,y,z)\equiv x^2+y^2+z^2-2xy-2yz-2zx\ ,$$

$$N_\lambda=[\Gamma(\alpha_i+\lambda+1)\Gamma(\alpha_i-\lambda+1)/\Gamma(2\alpha_i+1)]^{1/2}\ .$$

Then the vertex functions are the following:

Fermion vertex.

$$V_F(0;\tfrac12,\tfrac12)=-V(0;-\tfrac12,-\tfrac12)$$
$$=\frac12\left\{\left(\frac{-L^+}{4m_bm_d}\right)^{1/2}[2m_bm_d+L^+-\lambda_F/s_i-2\alpha_iL^+-s_i\alpha_i(\alpha_i-1)]\right.$$
$$\left.-\left(\frac{-L^-}{4m_bm_d}\right)^{1/2}2(m_b+m_d)^2\lambda_F^{-1/2}[\alpha_iL^++s_i\alpha_i(\alpha_i-1)]\right\}\ ,$$

$$V_F(1;\tfrac12,-\tfrac12)=-V(-1;-\tfrac12,\tfrac12)$$
$$=\frac12\left(\frac{-L^-}{4m_bm_d}\right)^{1/2}2\sqrt{t}(m_b+m_d)\lambda_F^{-1/2}[\alpha_iL^++s_i\alpha_i(\alpha_i-1)]\ ,$$

where $L^{\pm}=(m_b\pm m_d)^2-t$, $\lambda_F=L^+L^-$. All of the above expressions have been written for unequal fermion masses. In the particular study at hand $m_b=m_d$, of course.

A_1 vertex.

$$V_B(0;0,0)=-\frac{i}{\sqrt2}\left[-\lambda_B^{1/2}/(m_c\sqrt{s_i})+\sqrt{s_i}\,\alpha_i(t+m_c^2-m_a^2)/(m_c\lambda_B^{1/2})\right]\ ,$$

$$V_B(1;1,0)=V_B(-1;-1,0)=-\frac{i}{\sqrt2}[\sqrt{s_i}\,\alpha_i(2t)^{1/2}/\lambda_B^{1/2}]\ .$$

A_2 vertex.

$$V_B(0;0,0)=0\ ,$$

$$V_B(1;1,0)=-V_B(-1;-1,0)=(3\sqrt2\,i\lambda_B^{1/2}\alpha_i\sqrt{t})^{\frac12}[1/(m_cs_i)-(\alpha_i-1)(t+m_c^2-m_a^2)/(m_c\lambda_B)]\ ,$$

$$V_B(2;2,0)=-V_B(-2;-2,0)=(3\sqrt2\,i\lambda_B^{1/2}\alpha_i\sqrt{t})[-(\alpha_i-1)\sqrt{t}/\lambda_B]\ .$$

A_3 vertex.

$$V_B(0;0,0)=-\frac{1}{\sqrt6}\{\lambda_B/(2m_c^2s_i)-\alpha_i(t+m_c^2-m_a^2)/m_c^2+\alpha_i(\alpha_i-1)s_i[(t+m_c^2-m_a^2)^2+2m_c^2t]/(2m_c^2\lambda_B)\}\ ,$$

$$V_B(1;1,0)=V_B(-1;-1,0)=-\tfrac12[-\alpha_i\sqrt{t}/m_c+s_i\alpha_i(\alpha_i-1)\sqrt{t}(t+m_c^2-m_a^2)/(m_c\lambda_B)]\ ,$$

$$V_B(2;2,0)=V_B(-2;-2,0)=-\tfrac12[s_i\alpha_i(\alpha_i-1)t/\lambda_B]\ .$$

Now to the details of the continuation. The path of the analytic continuation used, the Trueman-Wick path,[18] is shown on the physical-region plot of Fig. 3. Along the full-line segment of the path $t(s)$ has a small positive (negative) imaginary part, while along the dashed line segment $t(s)$ has a small negative (positive) imaginary part. The behavior of the vertex functions displayed above under this continuation can easily be deduced from the behavior of the following functions upon which they depend:

$$\sqrt{t} \to -i\sqrt{-t}, \quad \sqrt{-s} \to i\sqrt{s}, \quad \lambda^{1/2} \to \lambda^{1/2}, \quad (-L^{\pm})^{1/2} \to \pm i(L^{\pm})^{1/2} .$$

[It might be worth noting at this point that the complex conjugation indicated in (2) is done *before* the analytic continuation is carried out.]

In addition, after analytic continuation and after letting $s \to \infty$,

$$\mathfrak{D}^{\alpha_i}_{\mu\nu}(\phi, \theta, -\phi)^* \to \{i^{-\mu} e^{i\mu\phi}[(t - t_{\min})/t]^{|\mu|/2}(-2t/\lambda_F)^{\alpha_i/2}/N_\mu\} \times \{i^{\nu} e^{-i\nu\phi}[(t - t_{\min})/t]^{|\nu|/2}(-2t/\lambda_F)^{\alpha_i/2}/N_\nu\}(-s/2)^{\alpha_i} , \tag{3}$$

where

$$t_{\min} = (1/2s)[2(m_a^2 m_d^2 + m_c^2 m_b^2) - (s - m_a^2 - m_b^2)(s - m_c^2 - m_d^2) + \lambda(s, m_a^2, m_b^2)^{1/2}\lambda(s, m_c^2, m_d^2)^{1/2}] .$$

To derive this result first write

$$\mathfrak{D}^J_{\mu\nu}(\phi, \theta, -\phi)^* = e^{i\mu\phi} d^J_{\mu\nu}(\theta) e^{-i\nu\phi} .$$

Then, assuming for the moment that $\nu \geq \mu \geq 0$, use Eq. (A1) of Jackson and Hite[19] to write

$$d^J_{\mu\nu}(\theta) = \frac{(\sin\tfrac{1}{2}\theta)^{\nu-\mu}(\cos\tfrac{1}{2}\theta)^{\nu+\mu}\mathcal{P}_\nu(\cos\theta)}{[(J+\mu)!(J-\mu)!(J+\nu)!(J-\nu)!]^{1/2}} ,$$

where

$$\mathcal{P}_\nu(\cos\theta) = \sum_{i=0}^{J-\nu} \binom{J-\nu}{i} \frac{(J+\nu+i)!(J-\mu)!}{2^i(\nu-\mu+i)!} (\cos\theta - 1)^J$$

is a polynomial in $\cos\theta$.

By straightforward manipulations

$$d^J_{\mu\nu}(\theta) = \left(\frac{\sin\theta}{\cos\theta}\right)^{\mu+\nu}\left(\frac{\cos\theta}{1-\cos\theta}\right)^{\mu} (\tfrac{1}{2}\cos\theta)^{\nu}\mathcal{P}_\nu(\cos\theta)/[N_\mu N_\nu (2J)!] ,$$

where N_μ, N_ν were defined earlier.

To discuss the analytic continuation of $d^J_{\mu\nu}(\theta)$, expressions for $\sin\theta$ and $\cos\theta$ in terms of s and t are needed. These are[19]

$$\cos\theta = [2t(s - m_a^2 - m_b^2) + (t + m_a^2 - m_c^2)(t + m_b^2 - m_d^2)]/\lambda_B^{1/2}\lambda_F^{1/2} \equiv \eta(s,t)/\lambda_B^{1/2}\lambda_F^{1/2} ,$$

$$\sin\theta = (2tL)^{1/2}/\lambda_B^{1/2}\lambda_F^{1/2} ,$$

where L is the Kibble function[20]

$$L = \begin{pmatrix} 2m_a^2 & s + m_a^2 - m_b^2 & t - m_a^2 - m_c^2 \\ s + m_a^2 - m_b^2 & 2s & m_d^2 - m_c^2 - s \\ t - m_a^2 - m_c^2 & m_d^2 - m_c^2 - s & 2m_c^2 \end{pmatrix} .$$

Under the chosen path of analytic continuation $L^{1/2} \to L^{1/2}$, and so the behavior of $\cos\theta$ and $\sin\theta$ under analytic continuation is

$$\cos\theta \to \eta/\lambda_B^{1/2}\lambda_F^{1/2} = \text{original expression for } \cos\theta ,$$

$$\sin\theta \to -i(-2tL)^{1/2}/\lambda_B^{1/2}\lambda_F^{1/2} .$$

Thus, under analytic continuation,

$$d^J_{\mu\nu}(\theta) \to (-i)^{\mu+\nu}\left[\frac{(-2tL)^{1/2}}{\eta}\right]^{\mu+\nu}\left(\frac{\cos\theta}{1-\cos\theta}\right)^{\mu} (\tfrac{1}{2}\cos\theta)^{\nu}\mathcal{P}_\nu(\cos\theta)/[N_\mu N_\nu (2J)!] .$$

If now the large-s limit is taken

$$\cos\theta \to 2ts/\lambda_B^{1/2}\lambda_F^{1/2}\ , \qquad L \to -2(t-t_{\min})s^2\ , \qquad \mathcal{P}_\nu(\cos\theta) \to (2J)!\,(\tfrac{1}{2}\cos\theta)^{J-\nu}\ ,$$

yielding, under analytic continuation and $s \to \infty$,

$$d^J_{\mu\nu}(\theta) \to i^{\nu-\mu}[(t-t_{\min})/t]^{(|\mu|+|\nu|)/2}(ts/\lambda_B^{1/2}\lambda_F^{1/2})^J/N_\mu N_\nu\ . \tag{4}$$

By using the symmetries of the d functions[21] Eq. (4) can be shown to hold for all μ, ν. It is a simple matter then to reach Eq. (3).

IV. ANALYTICALLY CONTINUED t-CHANNEL AMPLITUDES

After carrying out the analytic continuation specified in the preceding section and subsequently letting $s \to \infty$, the amplitudes (2) are found to have the form (for all A mesons)

$$\mathfrak{M}^{(i)\nu}_{\tau\sigma}(s,t) \to -\mathfrak{B}_i(\nu)\mathfrak{F}_i(\tau,\sigma)\frac{1}{s_i}\,\frac{\pi\alpha_i}{\sin\pi\alpha_i}\,\frac{\cos\frac{1}{2}\pi\alpha_i}{\Gamma(1+\alpha_i)}\,e^{-i(\pi\alpha_i/2)}(s/s_i)^{\alpha_i}\ , \tag{5}$$

where the residue functions $\mathfrak{B}_i(\nu)$ and $\mathfrak{F}_i(\tau,\sigma)$ are the following:

Fermion vertex.

$$\mathfrak{F}_i(\tfrac{1}{2},\tfrac{1}{2}) = -\mathfrak{F}_i(-\tfrac{1}{2},-\tfrac{1}{2}) = \frac{i}{2}\left\{\left(\frac{L^+}{4m_bm_d}\right)^{1/2}[2m_bm_d + L^+ - \lambda_F/s_i - 2\alpha_iL^+ - s_i\alpha_i(\alpha_i-1)] + \left(\frac{L^-}{4m_bm_d}\right)^{1/2}2(m_b+m_d)^2\lambda_F^{-1/2}[\alpha_iL^+ + s_i\alpha_i(\alpha_i-1)]\right\}\ ,$$

$$\mathfrak{F}_i(\tfrac{1}{2},-\tfrac{1}{2}) = \mathfrak{F}_i(-\tfrac{1}{2},\tfrac{1}{2}) = -\frac{i}{2}\left\{\left(\frac{L^-}{4m_bm_d}\right)^{1/2}2(t_{\min}-t)^{1/2}(m_b+m_d)\lambda_F^{-1/2}[\alpha_iL^+ + s_i\alpha_i(\alpha_i-1)]\right\}\ .$$

A_1 vertex.

$$\mathfrak{B}_i(0) = -\frac{i}{\sqrt{2}}\left[-\lambda_B^{1/2}/(m_c\sqrt{s_i}) + \sqrt{s_i}\,\alpha_i(t+m_c^2-m_a^2)/(m_c\lambda_B^{1/2})\right]\ ,$$

$$\mathfrak{B}_i(1) = -\mathfrak{B}_i(-1) = \frac{i}{\sqrt{2}}[\sqrt{2}\sqrt{s_i}\,\alpha_i(t_{\min}-t)^{1/2}/\lambda_B^{1/2}].$$

A_2 vertex.

$$\mathfrak{B}_i(0) = 0\ ,$$

$$\mathfrak{B}_i(1) = \mathfrak{B}_i(-1) = -(3\sqrt{2}i)(t_{\min}-t)^{1/2}\lambda_B^{1/2}\tfrac{1}{2}[1/(m_cs_i) - (\alpha_i-1)(t+m_c^2-m_a^2)/(m_c\lambda_B)]\ ,$$

$$\mathfrak{B}_i(2) = -\mathfrak{B}_i(-2) = -(3\sqrt{2}i)\lambda_B^{-1/2}(t_{\min}-t)(\alpha_i-1)\ .$$

A_3 vertex.

$$\mathfrak{B}_i(0) = -\frac{1}{\sqrt{6}}\{\lambda_B/(2m_c^2s_i) - \alpha_i(t+m_c^2-m_a^2)/m_c^2 + \alpha_i(\alpha_i-1)s_i[(t+m_c^2-m_a^2)^2 + 2m_c^2t]/(2m_c^2\lambda_B)\}\ ,$$

$$\mathfrak{B}_i(1) = -\mathfrak{B}_i(-1) = \tfrac{1}{2}(t_{\min}-t)^{1/2}[-\alpha_i/m_c + s_i\alpha_i(\alpha_i-1)(t+m_c^2-m_a^2)/(m_c\lambda_B)]\ ,$$

$$\mathfrak{B}_i(2) = \mathfrak{B}_i(-2) = -\tfrac{1}{2}s_i\alpha_i(\alpha_i-1)(t_{\min}-t)/\lambda_B\ .$$

In writing down these residue functions the choice $\phi = \pi$ was made in (2) (see Fig. 2). This corresponds to using the s-channel Gottfried-Jackson frame[22] for the continued amplitudes, $\vec{p}_c = 0$, $\vec{p}_a$ along the $+z$ axis and $\vec{p}_b \times \vec{p}_d$ along the $+y$ axis. In terms of $f^\nu_{\tau\sigma}(s,t)_c$ [the amplitudes of (1) after analytic continuation] the differential cross section and t-channel SDME are

$$\frac{d\sigma}{dt} = \frac{m_bm_d}{4\pi}\,\frac{1}{\lambda(s,m_a^2,m_b^2)}\,\frac{1}{2J_b+1}\sum_{\sigma,\tau,\nu}|f^\nu_{\tau\sigma}(s,t)_c|^2\ ,$$

$$\rho ij(s,t) = \sum_{\sigma,\tau} f^i_{\tau\sigma}(s,t)_c f^j_{\tau\sigma}(s,t)^*_c \Big/ \sum_{\sigma,\tau,\nu} f^\nu_{\tau\sigma}(s,t)_c f^\nu_{\tau\sigma}(s,t)^*_c\ .$$

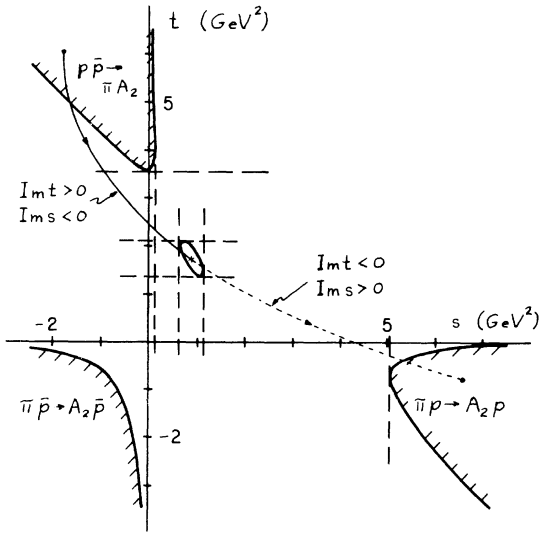

FIG. 3. The physical regions of $\pi p \to A_2 p$ and its crossed reactions. Those for A_1 and A_3 production are qualitatively similar. The solid curve, bounding these regions and the central unphysical loop, is given by the vanishing of the Kibble function, $\Delta = 0$. Tangent lines to this curve are shown dotted. The tangent lines bounding the small central loop are given by $\lambda(t, m_a^2, m_c^2) = 0$ and $\lambda(s, m_a^2, m_b^2) = 0$. The remaining tangent lines are given by $\lambda(t, m_b^2, m_d^2) = 0$ and $\lambda(s, m_c^2, m_d^2) = 0$. Also shown is the real projection of the Trueman-Wick path of analytic continuation from the t-channel to the s-channel physical region.

The parameters s_i in (5) and in the residue functions $\mathcal{B}_i$ and $\mathcal{F}_i$ were identified in[13] as the inverse of the common slope of the linear Regge trajectories of the external particles and the exchanged particles. For the f-exchange amplitudes [$i = f$ in (5)] the choices

$$s_f = 1.0 \text{ GeV}^2, \quad \alpha_f(t) = t + 0.40$$

are made. For the P-exchange amplitudes [$i = P$ in (5)] s_P is interpreted simply as a parameter, perhaps loosely related to the inverse slope of the P trajectory. In any case the choices

$$s_P \to \infty, \quad \alpha_P = 1.0, \quad G_P \to G_P s_P^n$$

($n = \frac{3}{2}$, 3, 2 for A_1, A_2, A_3, respectively) are made. The factors s_P^n were added solely to keep the P-exchange amplitudes finite as $s_P \to \infty$. Some features of the amplitudes worth noting at this point are that the helicity amplitude $\lambda = 0$ ($\lambda = \pm 1$) dominates for A_1 and A_3 (A_2) production and that $B_P(0)$ differs in sign from $B_f(0)$ for $t \lesssim 0$. This latter feature has consequences, to appear shortly, insofar as the phase ϕ_P in (1) is concerned.

TABLE II. Parameters of Eq. (1) used in fitting the data with Pomeron and f-meson exchange. Unbracketed numbers refer to the incoherent model; bracketed numbers refer to the conventional model. σ^P (σ^f) is the cross section due to P (f) exchange alone.

Meson	G_P	G_f	B (GeV^{-2})	σ^P/σ^f at 16 GeV/c
A_1	38	270	6.5	1.3
	[32]	[230]	[6.0]	[1.4]
A_2	8	35	5.0	2.4
	[7]	[30]	[4.7]	[2.8]
A_3	32	200	5.2	1.9
	[25]	[180]	[4.8]	[1.6]

V. FITS TO PARTIAL-WAVE-ANALYZED DATA

The model is specified by inserting the amplitudes (5) into (1) thus leaving the four parameters G_P, G_f, B, and ϕ_P to be adjusted to fit the data. Of course, in conventional Regge-pole theory ϕ_P is not free but is specified uniquely. Nevertheless when the conventional choice failed to give completely successful fits to the data several other possibilities for ϕ_P were considered.

Initially, in an attempt to get an estimate of the size of the parameters, fits were sought under the assumption that the P and f contributions to all

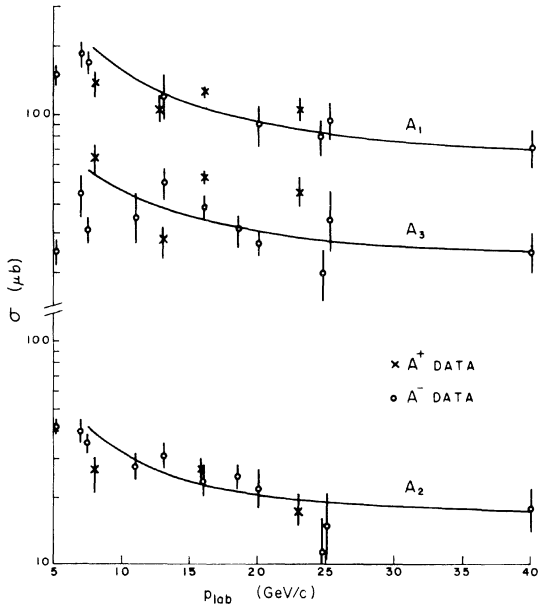

FIG. 4. Energy dependence of the cross sections for A_1, A_2, and A_3 production with 3π mass intervals 1.0–1.2 GeV/c^2 for A_1, 1.2–1.4 GeV/c^2 for A_2, 1.5–1.8 GeV/c^2 for A_3. The solid curve is a theoretical curve with parameters chosen to fit the data.

helicity amplitudes are incoherent: that is, that all interference terms between $\mathfrak{M}^{(P)}$ and $\mathfrak{M}^{(f)}$ vanish. This makes ϕ_P redundant and leads to simple forms for observables:

$$d\sigma/dt = d\sigma^P/dt + d\sigma^f/dt$$

for differential cross sections and

$$\rho_{ij} = (\rho_{ij}{}^P d\sigma^P/dt + \rho_{ij}{}^f d\sigma^f/dt)/(d\sigma/dt)$$

for SDME, where a superscript P (f) indicates the contribution to the observable due to P (f) exchange alone.

In addition, tentative assumptions were made that $d\sigma^P/dt = \text{const} \times e^{2Bt}$ for A_1 and A_3 production and $d\sigma^P/dt = \text{const} \times te^{2Bt}$ for A_2 production. This allowed fits to the total cross section at two energies and to the differential cross section at one energy to be made by hand for each of the A mesons and led to preliminary values for the parameters. Some final variations of the parameters were then made in order to get reasonable eyeball fits to most of the data. These final values are given in Table II as unbracketed numbers (taking masses in GeV/c^2, s and t in GeV^2, and σ in μb). Variations from these values by some 10% will give comparable fits.

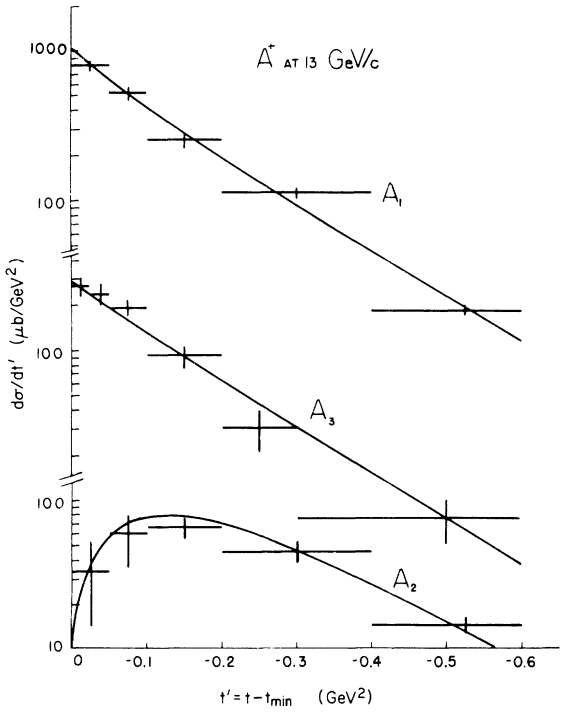

FIG. 5. Differential cross sections for A^+ production at 13-GeV/c π^+ laboratory momentum. In each case, the data has been normalized to the total cross section given by the solid curve of Fig. 4.

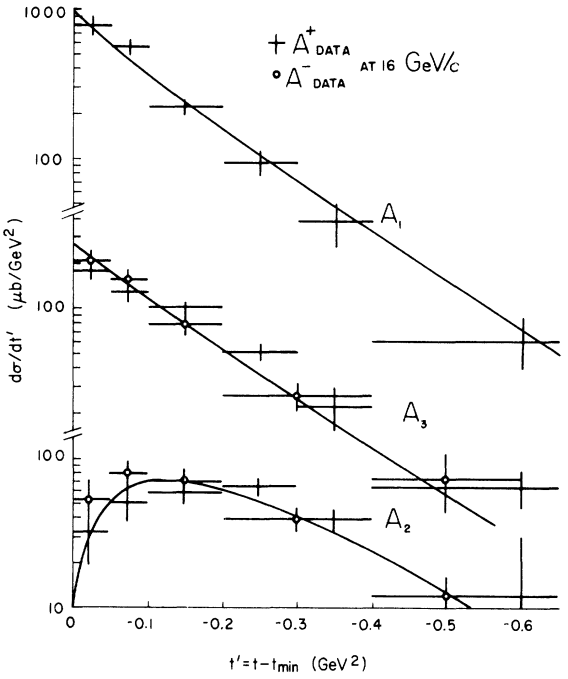

FIG. 6. The solid curves are calculated differential cross sections for A-meson production at 16 GeV/c. The data points are averages over runs at several energies; 8, 16, and 23 GeV/c for A^+, 11–25 GeV/c for A^-. In each case the data has been normalized to the total cross section at 16 GeV/c given by the appropriate solid curve of Fig. 4.

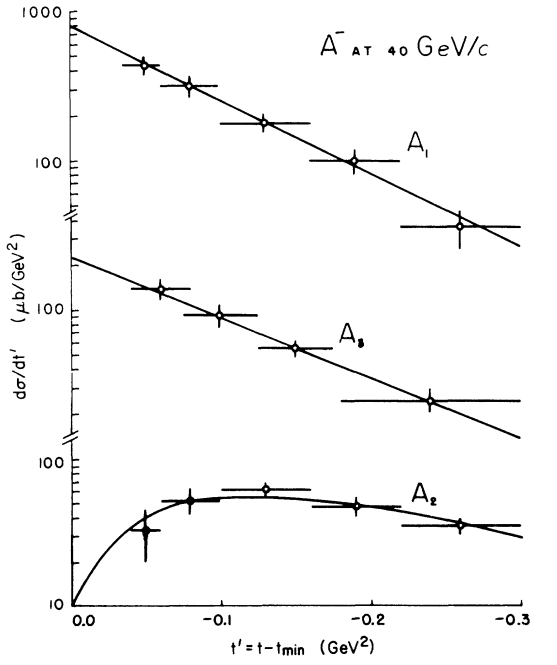

FIG. 7. Differential cross sections for A^- production at 40 GeV/c.

The partial-wave-analyzed data used and the fitted curves resulting from the incoherent model are shown in Figs. 4–12. With the exception of $\rho_{11} \simeq \frac{1}{2}(1-\rho_{00})$ for A_1 and A_3 and $\rho_{22} \simeq \frac{1}{2}(1-2\rho_{11})$ for A_2, all SDME not shown, including their imaginary parts, were calculated to be small or zero and are consistent with the experimental values of zero (within experimental error). The only pronounced disagreement between theory and experiment occurs in the sign, but not in the magnitude, of $\mathrm{Re}\rho_{12}$ for A_2 and $\mathrm{Re}\rho_{10}$ for A_3.

Using the values of G_P, G_f, and B secured above, the conventional Regge model was adopted: $\phi_P = 0$ for A_2, $\phi_P = \pi$ for A_1 and A_3. With these phase choices the Pomeron contribution to the dominant helicity amplitude carries the phase factor $e^{-i(\pi/2)}$ while the f contribution carries the phase factor $e^{-i(\pi\alpha_f/2)}$. Some modification in the sizes of the parameters were found to be necessary in order to obtain good eyeball fits to the data; the new values are displayed in Table II as bracketed numbers. The curves obtained using this conventional model are substantially the same as those exhibited in the figures and therefore are not shown. The only notable differences are that the wiggles in the A_1 curves of Figs. 8 and 9 are smoothed out and that the values for the imaginary parts of ρ_{10} in the A_1 and A_3 cases are so large as to lie just outside the

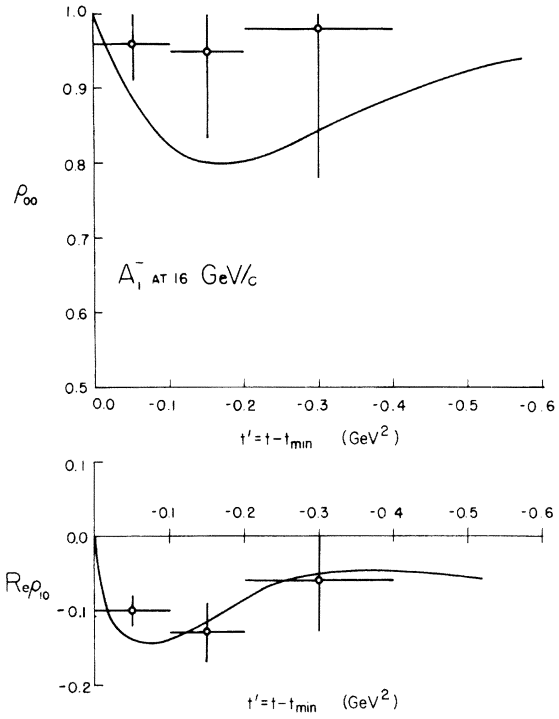

FIG. 9. Spin density matrix elements of the A_1^-. The solid curves are calculated for 16-GeV/c π^- laboratory momentum. The data points are averages over runs at several energies from 11 to 25 GeV/c.

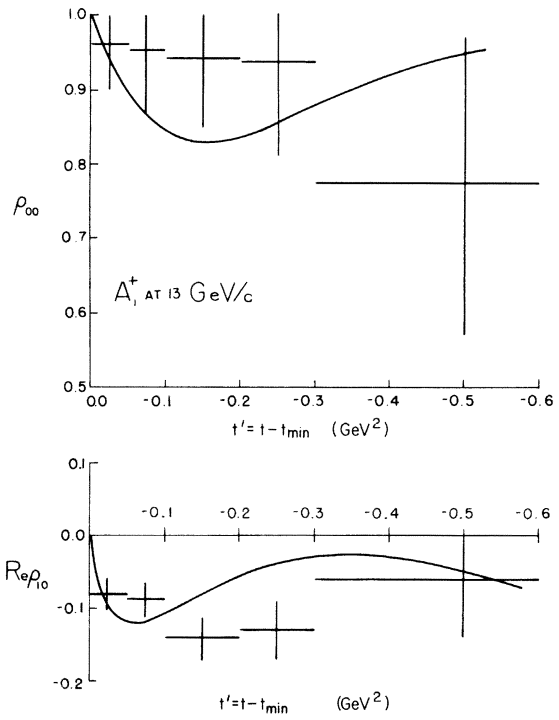

FIG. 8. Spin density matrix elements of the A_1^+ at 13 GeV/c.

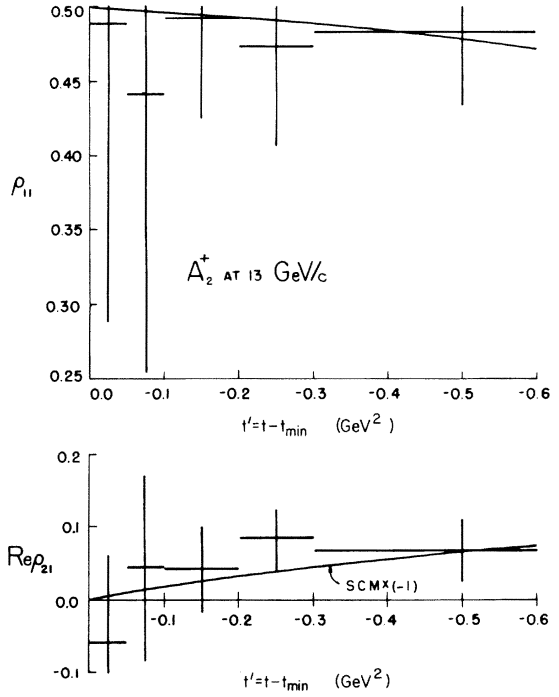

FIG. 10. Spin density matrix elements of the A_2^+ at 13 GeV/c. The calculated $\mathrm{Re}\rho_{12}$ has been reversed in sign in this plot.

rather generous experimental errors. By far the most important point to be made is that the calculated $\mathrm{Re}\rho_{12}$ for A_2 and $\mathrm{Re}\rho_{10}$ for A_3 are still opposite in sign to the analyzed data. [In passing it might be remarked that it is not difficult to see why the conventional model and the incoherent model agree so well with each other. For large values of $(-t)$, say, around 0.4 GeV^2, the P and f amplitudes are out of phase by 90° while for small values of $(-t)$ the P contribution is dominant. Thus the interference term between the P and f amplitudes in the conventional model tends to be small.]

Several other possibilities for ϕ_P were tried in unsuccessful attempts to see if *all* calculated curves could be brought into agreement with the data. For example, neither constraining the P and f contributions to the dominant helicity amplitudes at $t \leq 0$ to be exactly in phase with each other or to be exactly out of phase with each other worked. Furthermore, using a Pomeron with nonzero slope was unsuccessful also, as could be anticipated by a careful inspection of the residue functions $\mathcal{B}_i$ of (5).

As independent confirmation of the discrepancy between theory and experiment regarding the sign of $\mathrm{Re}\rho_{10}$ for A_3 the study by Ascoli *et al.*[11] of a Reggeized Deck model for A_1 and A_3 production may be cited. From Table I of Ref. 11 the s-channel production amplitudes at $t = -0.05$ GeV^2 for A-meson polarizations $M = 0$ and $M = 1$, evaluated in the Gottfried-Jackson frame (with $\vec{p}_a$ as quantization axis) are exactly out of phase [see the column labeled $\frac{1}{2}(F_{++} + F_{--})$] for both A_1 and A_3 production. Thus $\mathrm{Re}\rho_{10} < 0$ for A_1 and A_3, in agreement with the present work. Notice that, although the ρ/f and A_1/A_3 masses are taken as 820 MeV/c^2 and 1100 MeV/c^2, respectively, in this table, a study of Eq. (2.13) of Ref. 11, from which the table was constructed, shows that use of the physical ρ/f and A_1/A_3 masses will not alter the conclusion that $\mathrm{Re}\rho_{10} < 0$. Perhaps this difficulty regarding $\mathrm{Re}\rho_{10}$ for A_3 is related to the difficulty[12] of obtaining good fits to the overall production-decay characteristics of the A_3 when using the Reggeized Deck model.

The question of absorptive corrections and whether they could reconcile theory and experiment might be raised at this point. However, this is not likely to be the answer to the dilemma. An inspection of the curves presented in the figures and of the amplitudes (5) shows a remarkable similarity between the A_1 and the A_3 helicity amplitudes, especially in the small-t region. It is then very difficult to see how absorption could change the sign, but not the magnitude, of $\mathrm{Re}\rho_{10}$ for A_3 pro-

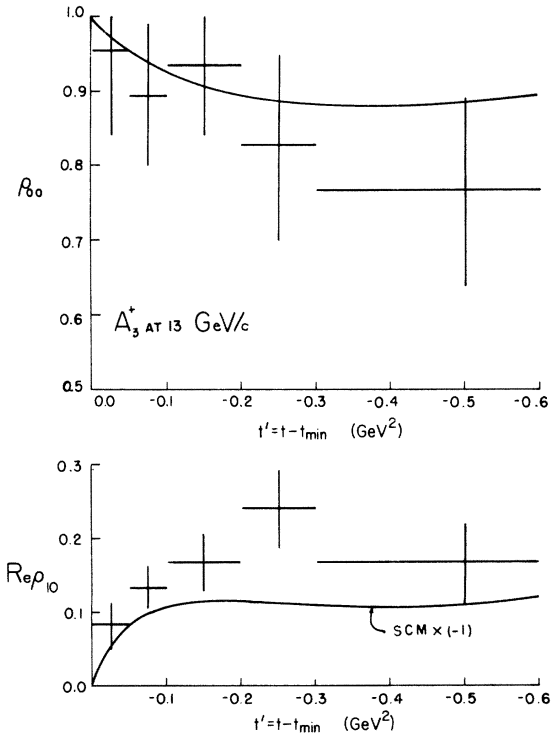

FIG. 11. Spin density matrix elements of the A_3^+ at 13 GeV/c. Note that the sign of $\mathrm{Re}\rho_{10}$ has been changed in making this plot.

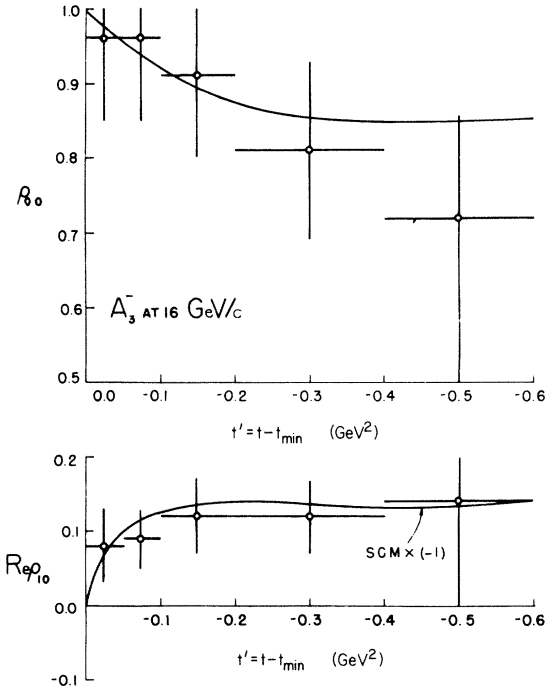

FIG. 12. Spin density matrix elements of the A_3^-. The solid curves are calculated for a π^- momentum of 16 GeV/c, while the data points are averages from runs at 11–25 GeV/c. The sign of the calculated $\mathrm{Re}\rho_{10}$ has been reversed in this plot.

duction while leaving the sign and the magnitude of the very similar quantity $\mathrm{Re}\rho_{10}$ for A_1 production unchanged.

VI. CONCLUSIONS

The simple t-channel model of A-meson production presented here with only Pomeron and f-meson exchanges accounts remarkably well for a substantial amount of data. Presumably this approach is correct in principle for A_2 *resonance* production. It is perhaps surprising how well it agrees with data on the production of the *threshold enhancements* A_1 and A_3. The only serious conflicts found with the data fitted are in the signs of two spin density matrix elements, one for each of the spin-2 mesons. Until the source of this disagreement is understood, it does not seem worthwhile to pin the model down in greater detail, e.g., to add some ρ-meson exchange, to study the imaginary parts of the SDME more carefully, etc.

In view of the discussion in the preceding section two possible conclusions concerning these discrepancies come readily to mind: (a) Conventional Regge-pole theory, *using residues extracted from a dual amplitude,* offers an incorrect description of the production characteristics of the spin-2 mesons A_2 and A_3, or (b) some assumption underlying the partial-wave analysis of the experimental data for A_2 and A_3 production is faulty.

Should (a) prove to be the case, it will also be necessary to explain why the Reggeized Deck model fails to give $\mathrm{Re}\rho_{10} > 0$ for A_3 production. Just where in fact to look for the source of the discrepancies found between theory and analyzed data is not clear at the moment.

Finally it is perhaps worth remarking that the model as presented above cannot give the observed phase difference[3] between the A_1 and A_2 production amplitudes. As pointed out in Ref. 3 a successful theoretical accounting of this phase difference in the Reggeized Deck model of A_1 production depends crucially on the signature factor in the propagator of the exchanged pion. There is no such factor in the present model. Furthermore, the Reggeized Deck model goes beyond what was developed above because it deals with the $\rho\pi$ "final" state of the A_1, while in the present model the propagation and decay mechanisms of the A_1 were not specified. Such phase questions have to be addressed ultimately of course if the present models of A_1 and A_3 production are to be taken seriously.

ACKNOWLEDGMENT

The assistance of Christopher C. Gerry in the early stages of this work is gratefully acknowledged.

[1]Particle Data Group, Rev. Mod. Phys. 48, S1 (1976).
[2]G. Ascoli *et al.*, Phys. Rev. D 7, 669 (1973).
[3]G. Ascoli *et al.*, Phys. Rev. Lett. 33, 610 (1974).
[4]Yu. M. Antipov *et al.*, Nucl. Phys. B63, 153 (1973); B76, 574E (1974).
[5]G. Thompson *et al.*, Phys. Rev. D 9, 560 (1974).
[6]G. Thompson *et al.*, Nucl. Phys. B69, 381 (1974).
[7]G. Otter *et al.*, Nucl. Phys. B80, 1 (1974).
[8]F. Wagner, M. Tabak, and D. M. Chew, Phys. Lett. 58B, 201 (1975); M. J. Emms *et al.*, *ibid.* 60B, 109 (1975).
[9]D. V. Brockway, thesis, AEC Report No. COO-1195--197, 1970 (unpublished).
[10]G. Ascoli *et al.*, Phys. Rev. Lett. 26, 929 (1971).
[11]G. Ascoli, L. M. Jones, B. Weinstein, and H. W. Wyld, Jr., Phys. Rev. D 8, 3894 (1973).
[12]G. Ascoli, R. Cutler, L. M. Jones, U. Kruse, T. Roberts, B. Weinstein, and H. W. Wyld, Jr., Phys. Rev. D 9, 1963 (1974).
[13]R. A. Morrow, Ann. Phys. (N.Y.) 88, 472 (1974).
[14]R. T. Deck, Phys. Rev. Lett. 13, 169 (1964).
[15]R. Carlitz, M. B. Green, and A. Zee, Phys. Rev. D 4, 3439 (1971).
[16]Chan Hong-Mo, Phys. Lett. 28B, 425 (1969); Chan Hong-Mo and Tsou Sheung Tsun, *ibid.* 28B, 485 (1969).
[17]C. Michael, Nucl. Phys. B63, 431 (1973).
[18]T. L. Trueman and G. C. Wick, Ann. Phys. (N.Y.) 26, 322 (1964).
[19]J. D. Jackson and G. E. Hite, Phys. Rev. 169, 1248 (1968).
[20]T. W. B. Kibble, Phys. Rev. 117, 1159 (1960).
[21]A. R. Edmonds, *Angular Momentum in Quantum Mechanics* (Princeton Univ. Press, Princeton, N.J., 1957), p. 60.
[22]K. Gottfried and J. D. Jackson, Nuovo Cimento 33, 309 (1964).